

F. LÓPEZ-TEJEIRA<sup>1</sup>  
F.J. GARCÍA-VIDAL<sup>2</sup>  
L. MARTÍN-MORENO<sup>1,✉</sup>

# Normal-incidence scattering of surface plasmon polaritons by one-dimensional nanoindentations: a multimodal description

<sup>1</sup> Departamento de Física de la Materia Condensada-ICMA, Universidad de Zaragoza, 50009 Zaragoza, Spain

<sup>2</sup> Departamento de Física Teórica de la Materia Condensada, Universidad Autónoma de Madrid, 28049 Madrid, Spain

Received: 2 March 2007 / Accepted: 2 May 2007  
Published online: 21 June 2007 • © Springer-Verlag 2007

**ABSTRACT** In this paper a theoretical study is made on the scattering of surface plasmon polaritons by a finite periodic array of one-dimensional rectangular grooves. Our approach is based on a multimodal expansion technique. We have found that the geometrical parameters of the array can be properly tuned to achieve optimal performance of the structure either as a Bragg reflector or as a converter of surface plasmon polaritons into light. Most importantly, such functionalities can be fully achieved with a relatively small number of grooves.

PACS 73.20.Mf; 78.67.-n; 41.20.Jb

## 1 Introduction

According to our everyday experience, light is usually reflected by metals. However, the interaction between light and mobile surface charges may also lead to the emergence of electromagnetic (EM) excitations localized on metal–dielectric interfaces. These so-called surface plasmon polaritons (SPPs) are well known for concentrating EM fields in sub-wavelength volumes and guiding them through the surface of a metal [1]. Such capabilities have become critical due to their potential use in the implementation of sub-wavelength photonic circuits [2, 3].

Consequently, a great deal of attention has been recently devoted to the creation of optical elements for SPPs [4–9], as well as to the efficient coupling of freely-propagating light into and out of them. This requires a precise knowledge of the scattering coefficients of the dispersion centers (i.e. deviations from a flat metal–dielectric interface) placed in the path of surface plasmon polaritons. Although many theoretical works have studied the scattering of SPPs by rough surfaces, scattering from simple geometries is not so well known.

From the theoretical side, the calculation of EM fields on a metal surface in the optical regime is a well-defined but difficult problem. Although the macroscopic Maxwell equations very accurately govern the interaction of the EM fields with the solid, their solution is difficult due to the different ranges of length scales involved (system size, wavelength, skin depth

etc.). Several techniques have been applied to solve this problem, each of them with their advantages and drawbacks. Brute force attacks by means of Green dyadic technique [10–14] or the discrete dipole approximation [15–17], may provide virtually exact results, but both methods suffer from a large (quite often prohibitive) numerical cost associated with the inversion of huge matrices and the calculation of cumbersome integrals. Rayleigh expansion has also been extensively applied in the context of SPP scattering by either rough surfaces [18, 19] or simple objects [20–22]. However, the calculation of the scattering coefficients within this approximation requires dealing with a difficult integral equation [23, 24] from which physical insight is not easily inferred.

In a previous work [25], we analyzed the scattering of SPPs impinging at normal incidence on a finite array composed of rectangular grooves by means of a modal expansion technique. In the present paper, we provide further details on such calculations and extend our study to the case in which multiple modes inside each groove are considered. A detailed discussion on the role of the groove depth will be also presented.

## 2 Scattering of SPPs by surface inhomogeneities

Consider a monochromatic SPP along a metal–air interface impinging at normal incidence onto an inhomogeneity region. Let us assume that such inhomogeneities are due to variations in the surface profile. Suppose that the metal has a wavelength-dependent dielectric function  $\varepsilon(\lambda)$  and that the surface relief profile has a given functional form. Our recipe for the solution is then quite straightforward: we only have to expand the non-zero EM field components in terms of the incident SPP plus scattered field, apply boundary conditions all over the surface and solve the continuity equations in order to obtain the EM fields at any desired point.

Of course, this is a non-trivial issue for which some simplifications are mandatory. The first one is related to the boundary conditions: instead of the strict Maxwell boundary conditions, we make use of the so-called surface impedance boundary conditions (SIBC) [26], which assume that the skin depth is much smaller than any other length scale within the problem. Consequently, SIBC are only applicable when the dielectric function of the metal satisfies  $|\varepsilon(\lambda)| \gg 1$ . Hence, the continuity equation at the metallic surface is reduced to a sim-

✉ Fax: +34 976761229, E-mail: lmm@unizar.es

ple expression involving the tangential components of the EM fields :

$$\mathbf{F}_t(\mathbf{r}) \equiv \mathbf{E}_t(\mathbf{r}) - Z_s \mathbf{H}_t(\mathbf{r}) \times \mathbf{n}(\mathbf{r}) = 0, \quad (1)$$

where  $Z_s = \varepsilon(\lambda)^{-1/2}$  and  $\mathbf{n}(\mathbf{r})$  is the unitary vector normal to the surface directed into the metal half-space. As  $Z_s \rightarrow 0$ , the auxiliary field  $\mathbf{F}$  transforms into  $\mathbf{E}$  and (1) accounts for the boundary condition of a perfect conductor.

The second simplification relies on the way we implement the field expansion inside the grooves, which extends to real metals the mode matching or momentum technique previously developed within the perfect conductor approximation (PCA) [27, 28]. Within this framework, the EM fields inside the indentations are expanded in terms of an eigenfunction series, each term of which obeys the appropriate wave equations in both air and metal regions. The problem of finding such a basis is easily solved if PCA is assumed for the vertical walls, which is valid for indentations much wider than the skin depth. As far as fairly good results can be obtained [29] without overly complicating the theoretical treatment, we project EM fields onto PCA eigenfunctions, although further refinements have been proposed [30, 31]. Surface impedance boundary conditions are otherwise assumed for the horizontal surfaces.

Such formalism enables us to describe the scattering properties of an arbitrary set of rectangular indentations without any restriction over their position or aspect ratio, providing a very compact representation of the EM fields and simple expressions for the scattering magnitudes. By using this technique, we have already studied the SPP scattering for single [29] and periodic [25] defects. Here, we revisit that latter case by incorporating a multimodal implementation of the method.

## 2.1 A tight-binding-like system of equations

According to the technique mentioned above, the method of launching SPPs onto a set of indentations closely resembles the back-side illumination employed in some experimental works [32–35]. We consider a single slit flanked by a set of  $N$  indentations placed in the output surface of an infinite metallic film of thickness  $h$  (see Fig. 1). Eventually, the distance between the slit and indentations will be taken to be infinity so that the slit merely plays the role of a virtual SPP-launcher.

In the present work, we consider the simplest case of 1D subwavelength indentations (grooves). Additionally, we impose that the external illumination be uniform along the  $y$ -axis, so we restrict ourselves to the scattering of SPs impinging onto the grooves at normal incidence. In this way, the tangential components of the  $\mathbf{F}$  field at the openings of a given indentation of width  $a_i$  located at position  $x_i$  can be written in terms of its modal amplitudes  $\{E_\alpha, E'_\alpha\}$  as

$$\begin{cases} \mathbf{F}_t(\mathbf{r})|_{z=0} = \sum_\alpha E_\alpha \Phi^\alpha(x), \\ \mathbf{F}_t(\mathbf{r})|_{z=h} = \sum_\alpha E'_\alpha \Phi^\alpha(x), \end{cases} \quad (2)$$

where

$$\Phi_x^\alpha = A_{x\alpha} \cos \frac{\alpha\pi}{a_i} \left( x + \frac{a_i}{2} - x_i \right); \quad \Phi_y^\alpha = 0, \quad (3)$$

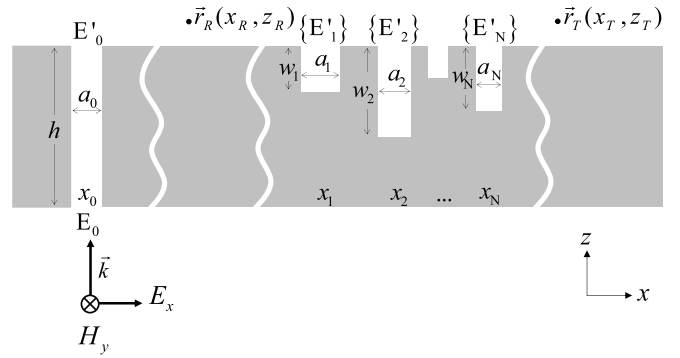


**FIGURE 1** Schematic picture of the system under study: single slit flanked in the output surface by an arbitrary set of  $N$  indentations located at a long distance from its right side. A  $p$ -polarized EM wave is impinging from the bottom. Parameters  $\{x_\alpha, a_\alpha, w_\alpha\}$  define the geometry of indentations

with  $A_{x0} = \sqrt{1/a_i}$  and  $A_{x\alpha} = \sqrt{2/a_i}$  for  $\alpha = 1, 2, \dots$ . By matching appropriately at the two interfaces, we obtain the full EM field in all spatial points as a function of the projection onto these waveguide eigenmodes at  $z = 0$  and  $z = h$ . The main end product of such expanding and matching is a set of algebraic equations for the modal amplitudes of the  $\mathbf{F}$  field which closely resembles the usual tight-binding formalism in solid-state physics but includes interaction up to all neighbors. For the sake of simplicity, let us assume that the illuminating slit falls within the width range in which the PCA description of vertical walls still holds [36] but only the lowest mode is relevant. With  $n_m$  being the number of considered modes inside each groove, we then have to solve a linear system of  $Nn_m + 2$  equations for the modal amplitudes at the input and output openings of the slit ( $E_0, E'_0$ ) and the output openings of the  $N$  grooves ( $\{E'_\alpha\}$ ):

$$\begin{cases} (G_{00} - \epsilon_0) E_0 - G_{v0} E'_0 = I_0, \\ (G_{\alpha\alpha} - \epsilon_\alpha) E'_\alpha + \sum_{\beta \neq \alpha} G_{\alpha\beta} E'_\beta - G_{v0} E_0 \delta_{\alpha 0} = 0. \end{cases} \quad (4)$$

This set of equations is basically the same as the one obtained within the PCA [27] for the modal amplitudes of the electric field. Therefore its physical meaning remains unchanged, although the expressions are slightly different due to the non-zero impedance  $Z_s$  at the metal surface:  $I_0$  represents the back-side illumination on the slit (which must be  $p$ -polarized in order to excite SPPs); the “self-energy”  $\epsilon_\alpha$  is related to the bouncing back and forth of the EM fields inside indentation  $\alpha$ . For the slit,

$$\epsilon_0 = -i \frac{e^{ik_0 h} (1 + Z_s) + e^{-ik_0 h} (1 - Z_s)}{e^{ik_0 h} (1 + Z_s)^2 - e^{-ik_0 h} (1 - Z_s)^2}, \quad (5)$$

whereas for a groove,

$$\epsilon_\alpha = -i Y_\alpha \frac{(1 + \varphi_\alpha)}{(1 - Z_s Y_\alpha - (1 + Z_s Y_\alpha) \varphi_\alpha)}, \quad (6)$$

with

$$\varphi_\alpha = e^{2ik_\alpha w_\alpha} \frac{(1 - Z_s Y_\alpha)}{(1 + Z_s Y_\alpha)}, \quad (7)$$

being  $w_\alpha$  the depth of the groove, and  $k_\alpha = \sqrt{k_0^2 - (\alpha\pi/a_\alpha)^2}$ ,  $k_0 \equiv 2\pi/\lambda$  and  $Y_\alpha = k_0/k_\alpha$ . The coupling between the two sides of the slit is taken into account by

$$G_{v0} = \frac{2i}{(e^{ik_0h}(1+Z_s)^2 - e^{-ik_0h}(1-Z_s)^2)}. \quad (8)$$

Finally,  $G_{\alpha\beta}$  corresponds to the coupling between modes, reflecting that mode  $\beta$  emits radiation that can be collected by mode  $\alpha$ :

$$G_{\alpha\beta} = \int_{x_i - \frac{a_j}{2}}^{x_i + \frac{a_j}{2}} dx \int_{x_j - \frac{a_j}{2}}^{x_j + \frac{a_j}{2}} dx' (\Phi_x^\alpha)^* G(x, 0; x', 0) \Phi_x^\beta, \quad (9)$$

with

$$G(x, z; x', z') = \frac{i}{\lambda} \int_{-\infty}^{+\infty} dk \frac{e^{i(k(x-x') + \sqrt{k_0^2 - k^2}(z-z'))}}{\sqrt{k_0^2 - k^2} + k_0 Z_s}. \quad (10)$$

## 2.2 Emergence of surface plasmons

From a mathematical point of view,  $G_{\alpha\beta}$  in (9) is the projection onto eigenmodes  $\alpha$  and  $\beta$  of a scalar Green function  $G(\mathbf{r}, \mathbf{r}')$  across the openings of the indentations at which each mode is located. As  $Z_s \rightarrow 0$ , (10) transforms into an integral representation of the 0th-order Hankel function of the first kind [28], thus recovering the PCA in the low-energy limit of our approach. Even within the SIBC approximation, we find that the PCA result is still valid for  $|x-x'| \ll \lambda$ . However, the presence of  $Z_s$  in (10) strongly modifies its long-distance behavior. By means of asymptotic analysis, we have found that, in the limit where  $|z-z'|, \lambda \ll |x-x'|$ , oscillatory contributions within the kernel of (10) mutually cancel but in the region close to the integrand singularities at  $k = \pm k_p$ , with  $k_p$  satisfying

$$\sqrt{k_0^2 - k_p^2} = -Z_s k_0. \quad (11)$$

This is, by the way, the SPP dispersion relation of a flat metal-dielectric interface within the SIBC. Therefore, the long distance EM coupling along the surface is due to SPPs even in the presence of absorption. Hence, the function  $G$  can be approximated as

$$G_{as}(x, z; x', z') = -\frac{k_0^2 Z_s}{k_p} e^{i(k_p|x-x'| - k_0 Z_s|z-z'|)}. \quad (12)$$

Comparison with the exact result in the optical regime shows that the asymptotic limit is already reached for distances of about  $\lambda$ . For example, in the case of silver at  $\lambda = 750$  nm, we find that  $G_{as}(\mathbf{r}, \mathbf{r}')$  differs from  $G(\mathbf{r}, \mathbf{r}')$  by less than 10% for  $|x-x'| \approx 2\lambda$  (see Fig. 2). It is this knowledge of long-distance EM coupling being mediated by surface plasmon polaritons that allows us to use the system in Fig. 1 for the analysis of SPP scattering.

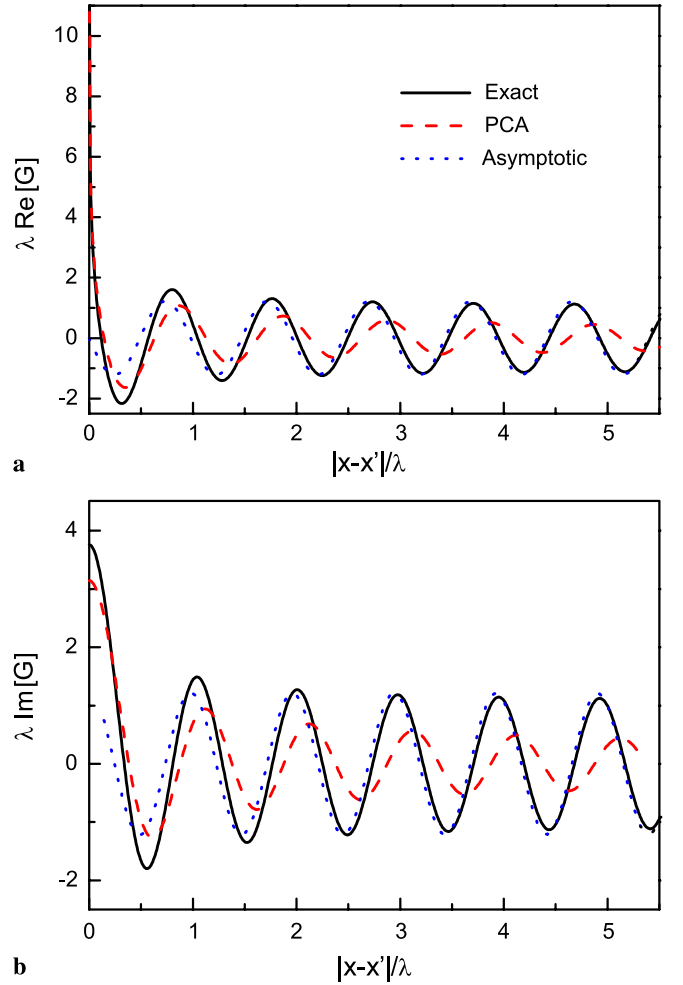


**FIGURE 2** Comparison between full calculation (*solid lines*), perfect conductor approximation (*dashed*) and asymptotic expansion (*dotted*) of the real (**a**) and imaginary (**b**) parts of  $\lambda G(x, 0; x', 0)$  as a function of distance at an air/Ag interface. Here  $\lambda = 750$  nm and  $Z_s = 1.338 \times 10^{-3} - 0.1975i$

## 2.3 Obtention of the scattering magnitudes

Let us now examine the term  $G_{0\alpha}E'_0$  in (4). According to (9), it can be interpreted as an illumination term originated by the EM field that the slit radiates onto the grooves. Thus, the equations governing the EM fields at the grooves become

$$(G_{\alpha\alpha} - \epsilon_\alpha)E'_\alpha + \sum_{\beta \neq \alpha, 0} G_{\beta\alpha}E'_\beta = \tilde{I}_\alpha, \quad (13)$$

where  $\tilde{I}_\alpha \equiv -G_{\alpha 0}E'_0$  are defined to resemble the back-side illumination  $I_0$ . The key point is that, according to (12), every  $\tilde{I}_\alpha$  corresponds to a SPP illumination on the mode  $\alpha$ , modulated by a constant factor that depends on the metal thickness, the intensity of the back illumination and the width of the slit. Within linear response, this factor is not relevant for the determination of scattering coefficients so the whole slit can then be treated as a theoretical artifact for SPP launching.

Once the self-consistent  $\{E'_\alpha\}$  are obtained, the calculation of the EM field in all space is straightforward, and therefore both the emittance  $S$  (which is the fraction of incoming SPP energy radiated into vacuum) and its angular distribution. As

the EM coupling between the grooves and a distant point on the surface is due to SPP, we can also obtain the SPP reflection ( $r$ ) and transmission ( $t$ ) amplitudes:

$$r = \sum_{\alpha=1}^N \varrho_{\alpha} e^{ik_p x_{\alpha}} E'_{\alpha}, \quad t = 1 + \sum_{\alpha=1}^N \tau_{\alpha} e^{-ik_p x_{\alpha}} E'_{\alpha}, \quad (14)$$

where

$$\varrho_{\alpha} = -i \frac{k_0^2 Z_s}{k_p} A_{\alpha\alpha} c_{\alpha}^*; \quad \tau_{\alpha} = -i \frac{k_0^2 Z_s}{k_p} A_{\alpha\alpha} c_{\alpha} \quad (15)$$

and

$$c_{\alpha} = \frac{a_{\alpha}}{2} \left[ e^{i\frac{\alpha\pi}{2}} \operatorname{sinc} \left[ \frac{a_{\alpha}}{2} k_p^- \right] + e^{-i\frac{\alpha\pi}{2}} \operatorname{sinc} \left[ \frac{a_{\alpha}}{2} k_p^+ \right] \right] \quad (16)$$

is a geometrical coefficient associated to each mode, with  $k_p^{\pm} = k_p \pm \alpha\pi/a_{\alpha}$ .

Notice that, if absorption is present,  $\operatorname{Im}[k_p] \neq 0$  and the SPP reflected and transmitted currents depend on the points ( $r_R, r_T$ ) at which the EM are evaluated, reflecting the absorption loss in the flat regions of the metal surface. This suggests that the scattering coefficients should be extracted from the EM fields at points close to the grooves, although in this case it is difficult to separate the diffractive contribution from the one due to SPPs. Nevertheless, provided that the grating lengths considered are shorter than the SPP absorption length, absorption can be neglected when computing the scattering magnitudes. In what follows, we present the results obtained under such assumption for finite periodic arrays of  $N$  identical rectangular grooves, patterned on a Ag film.

### 3 Scattering of SPPs by a finite periodic array of rectangular grooves

#### 3.1 Beyond the lowest mode approximation

In [25] we presented reflectance, transmittance and emittance curves of SPP scattering by different finite groove arrays consisting of identical rectangular grooves with width  $a = 100$  nm and depth  $w = 50$  nm separated by a period  $d$  of 600 nm. Those calculations were performed considering only the lowest mode inside each groove, which is quite reasonable for small  $a/\lambda$ . However, one may expect some corrections when including additional modes inside the indentations.

Figure 3a–c render the calculated reflectance  $R = |r|^2$ , transmittance  $T = |t|^2$  and emittance  $S$  spectra for the above-mentioned geometrical parameters in the case of a system composed of 10 grooves. Solid and dashed lines correspond respectively to lowest mode ( $\alpha = 0$ ) and multimodal (up to  $\alpha = 2$ ) expansions in (3). As can be seen, small differences arise between every pair of curves, which are only visible at the low- $\lambda$  edge of the spectra. Hence, both position and size of the spectral resonances within the working interval are very well described by the lowest mode approximation (LMA), as hypothesized in [25]. Within the working interval, no changes were observed when including additional modes. Consequently, a multimodal expansion up to  $\alpha = 2$  is adopted hereafter unless otherwise stated.

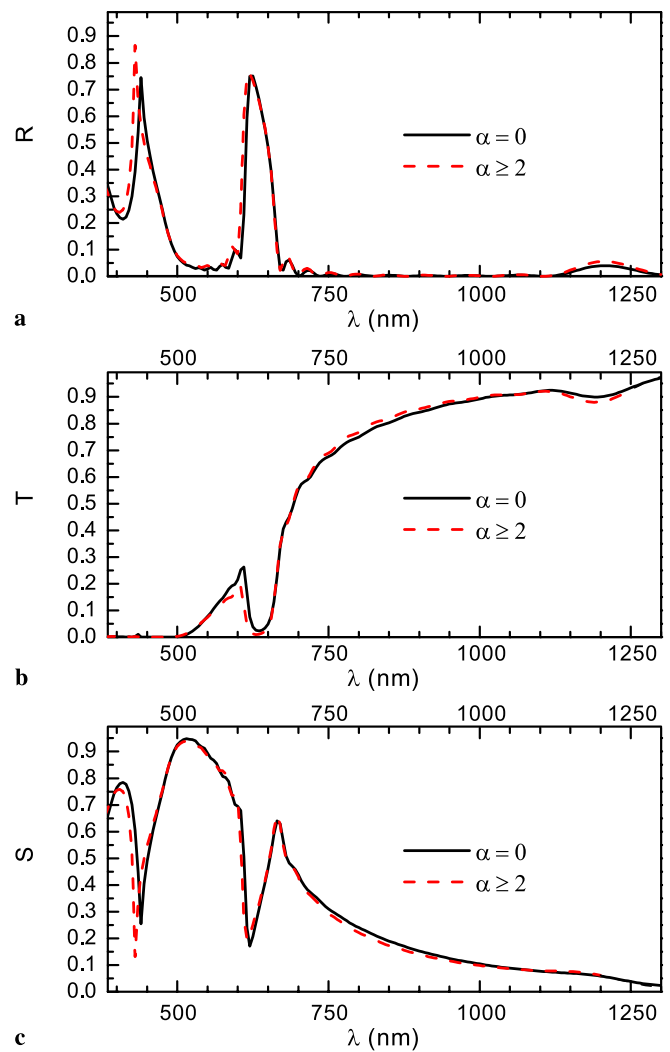


**FIGURE 3** Calculated  $R$  (a),  $T$  (b) and  $S$  (c) curves of SPP scattering by a finite periodic array consisting of 10 grooves on an Ag film. Here,  $a = 100$  nm,  $d = 600$  nm and  $w = 50$  nm. Solid lines correspond to the lowest mode ( $\alpha = 0$ ) and multimodal ( $\alpha \geq 2$ ) approximations respectively

#### 3.2 Resonant spectral features

Calculated  $R$ ,  $T$  and  $S$  spectra for increasing values of  $N$  are presented in Fig. 4a–c. In the case of a single groove (top panel),  $T$  increases with  $\lambda$ , while both  $R$  and  $S$  decrease. This is due to two mechanisms. First, there is a decrease of the relative size of the groove with respect to  $\lambda$ , which manifests in  $G_{\alpha\beta}$  scaling as  $(a/\lambda)$ . Second, as  $|\varepsilon(\lambda)|$  increases, the SPP is more extended in the air region and therefore less sensitive to the presence of obstacles at the surface. Panels b and c show how the addition of more grooves greatly modifies the optical response of the system.

As  $N$  increases, transmission gaps develop, as well as sharp resonances in both  $R$  and  $S$ . In order to gain insight into the origin of this behavior, it is helpful to analyze the EM surface modes of an infinite groove array. This can be readily done by looking for solutions to (13), imposing both  $\tilde{I}_{\alpha} = 0$  and Bloch theorem (i.e.  $E'_{\alpha} = E'e^{ik_x ad}$ ,  $k_x$  being the surface state wavevector at the given wavelength). The band structure (solid line) for surface modes in a periodic structure with

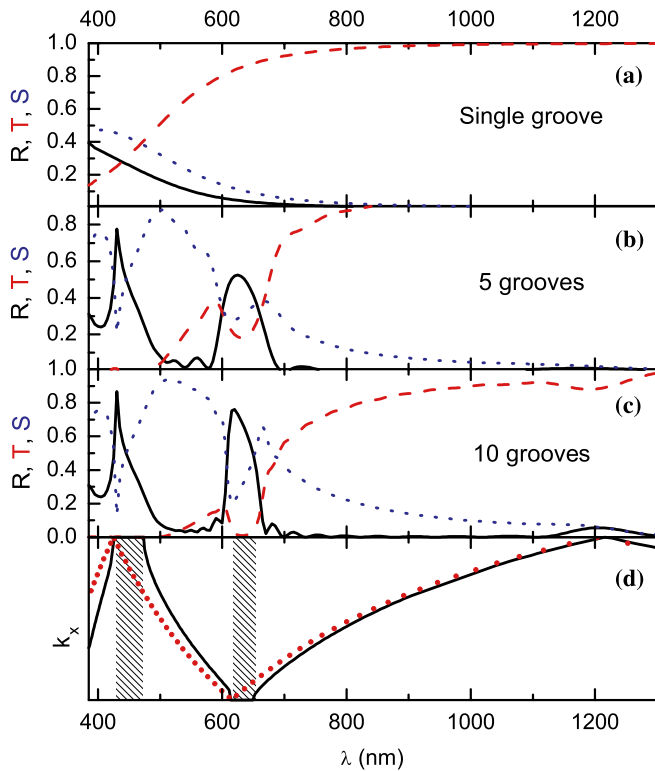


**FIGURE 4** Calculated  $R$  (solid),  $T$  (dashed) and  $S$  (dotted) curves of SPP scattering by a finite periodic groove array on a Ag film. Here,  $a = 100$  nm,  $d = 600$  nm and  $w = 50$  nm. Results in (a–c) correspond to structures with 1, 5 and 10 grooves respectively. Panel (d) shows the band structure (solid lines) for the same parameters as in (a–c) and the SPP dispersion relation in a flat air/Ag interface (dots). Gray-striped areas mark the photonic gaps

the same geometrical parameters as in (a) to (c) is presented in Fig. 4d, as well as the dispersion relation of SPPs in a flat air/silver interface (dots). As expected [37], band gaps occur with a low- $\lambda$  edge given by  $k_p d = m\pi$  with  $m = 1, 2, \dots$ , i.e. by the folding of the dispersion relation in a flat surface. On the contrary, the high- $\lambda$  edge depends on the geometry of the grooves, as it corresponds to a SPP standing wave with maxima at the groove positions. Evidently, spectral regions of low  $T$  in the finite array coincide with gaps in the band structure. Energy conservation implies a corresponding increase in  $R + S$ , but it is not obvious how this increase is divided between these two channels. However, there is a simple argument for the existence of reflection maxima. Let us consider the SPP wavefields emitted by two consecutive grooves in the region of reflection. There is an “optical path” phase difference of  $k_p d$  between these waves. Additionally, there is also a phase difference between emitters that is equal to  $k_x d$  in the case of a infinite system. But, as previously noted,

$$k_x d = k_p d = m\pi \quad (17)$$

at the low-wavelength gap edge so the SPP wavefields launched by all grooves interfere constructively (notice that they also interfere constructively in the transmission region, but not with the incident field). As  $\lambda$  is increased away from this condition, the constructive interference is progressively lost,  $R$  decreases and, for  $\lambda$  within the  $T$ -gap,  $S$  increases. If  $\lambda$  crosses the gap edge, the transmission channel is open, and

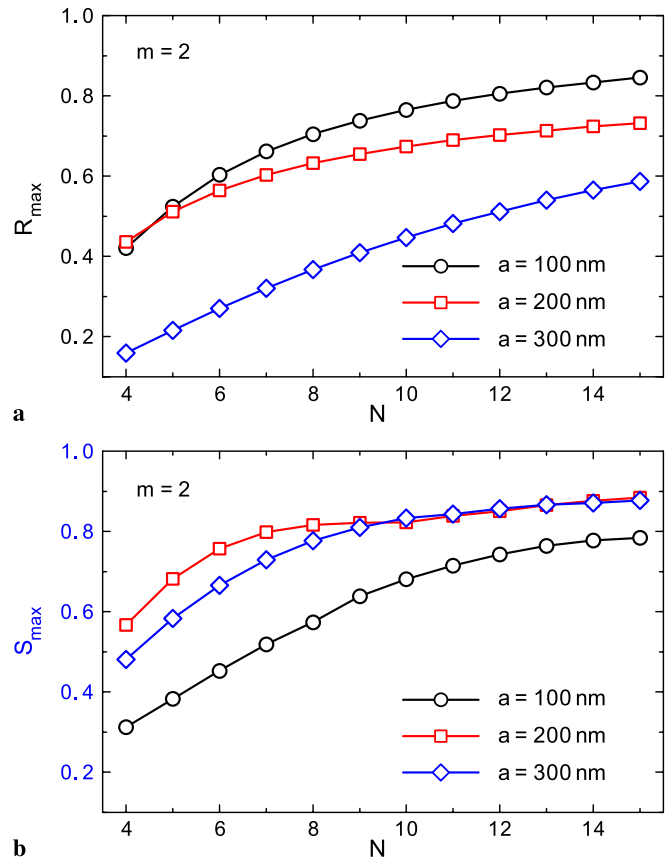


**FIGURE 5** Maximum values of  $R$  (a) and  $S$  (b) as a function of the number of grooves in the vicinity of  $k_p d = 2\pi$  for the same  $w, d$  as in Fig. 4 and increasing values of  $a$

$S$  decreases. Therefore,  $S$  presents peaks at the high- $\lambda$  edges of the gaps, as can be seen in Fig. 4. This mechanism explains the heuristic criterion for optimum mirror efficiency presented in [5] as well as the strong asymmetry in the positions of the reflectance peaks reported in [38].

Figure 5 renders the maximum  $R$  and  $S$  as a function of the number of grooves in the vicinity of  $k_p d = 2\pi$  for the same  $w$  and  $d$  parameters as in Fig. 4, and increasing values of the groove width. In order to reach convergence, additional modes have to be incorporated for  $a = 200, 300$  nm up to  $\alpha = 3$  and  $\alpha = 4$ , respectively. Please notice that a small number of indentations are sufficient to achieve either a large in-plane reflection or a high emission out of the plane. This rapid saturation is also consistent with [5]. With respect to the groove width, it clearly favors the out-of-plane efficiency of every single scatterer, increasing the total emittance at the expense of the mirror efficiency.

### 3.3 Dependence on groove depth

As the line of reasoning that leads us to the resonant condition of (17) does not take into account the role of the groove depth  $w$ , we find it worthwhile to analyze with some detail how the SPP scattering is influenced by this geometrical parameter. The dependence of  $R, T, S$  on groove depth is depicted in Fig. 6, for  $N = 10, a = 100$  nm and  $d = 600$  nm. As can be seen, the maxima of  $R$  at wavelengths satisfy-

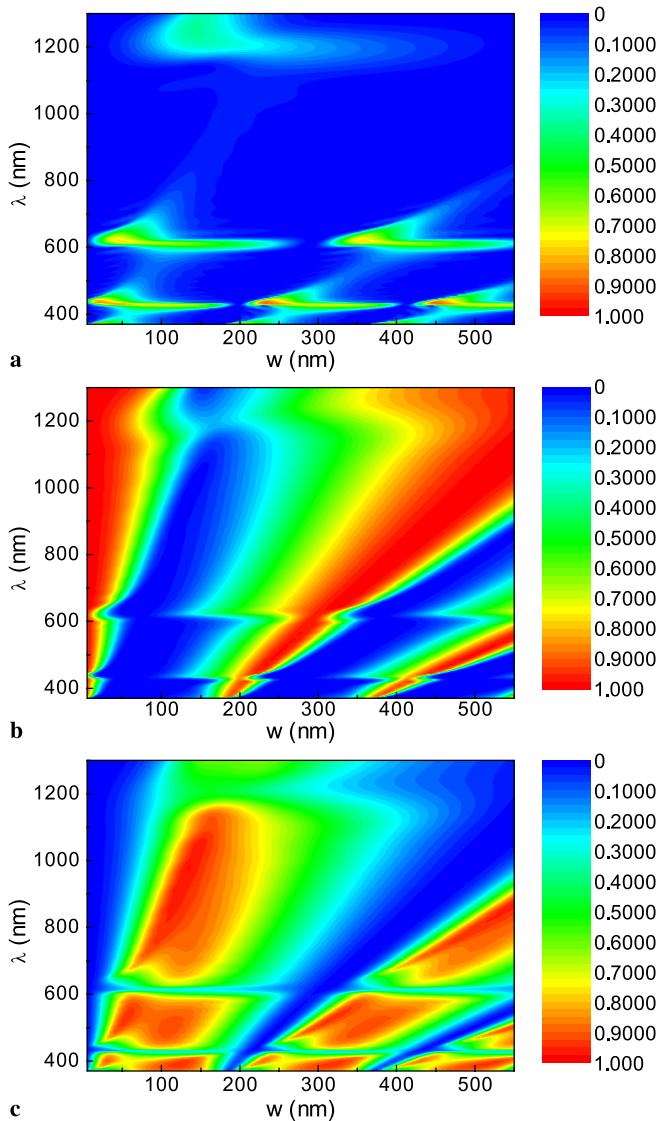


**FIGURE 6** Contour plots of  $R$  (a),  $T$  (b) and  $S$  (c) vs. both groove depth and wavelength for the same  $N$ ,  $a$ ,  $d$  as in Fig. 4c

ing  $k_p d = m\pi$  vary weakly on  $w$  for most ranges of groove depth. Such a weak dependence may be relevant for device design, considering that the control of  $w$  is often the most difficult point in groove fabrication. However, spectra show some extra features at resonant wavelengths that deserve further attention.

First of all, the reflection is very small at some values of  $w$  for which a maximum is expected according to (17). Simultaneously, at these groove depths,  $S \approx 0$  and  $T \approx 1$ . However, there also exist “hot-spots” for which  $R$  rises to a maximum well-above its average value within the depth interval. These fluctuations in the resonant behavior are directly related to the modal amplitudes  $\{E'_\alpha\}$  at the openings of the grooves, which depend on the interference between the incident field and the one that is reflected on the closed end of the indentation. Thus, a destructive interference results in the in-plane EM field being very small so no plasmon scattering takes place. As the optical response of the array then equals that of a flat surface, one could say that the grooves “become invis-

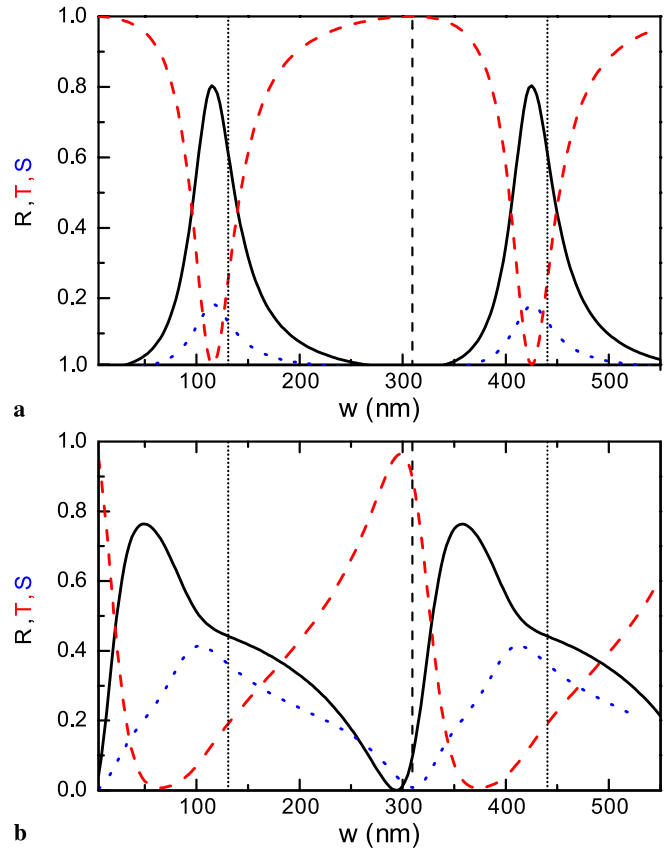


**FIGURE 7** Calculated  $R$  (solid),  $T$  (dashed) and  $S$  (dotted) vs. groove depth curves for a finite array composed of 10 grooves on an Ag film. Here,  $d = 600$  nm and  $\lambda = 619$  nm. Results in (a) and (b) correspond to structures with  $a = 10$  nm and  $a = 100$  nm, respectively. Vertical dashed (dotted) lines mark the condition for destructive (constructive) interference within the LMA

ible”. Conversely, constructive interference maximizes SPP scattering, being the in-plane vs out-of-plane ratio governed by the considerations presented in Sect. 3.2.

On the assumption of LMA, analytical expressions related to such interference processes can be found for grooves in the limit  $a/\lambda \rightarrow 0$ . We want to stress that this limit exceeds the range of validity of SIBC (see Sect. 2) and has only an academic value, as far as any realistic description should take into account the dependence of the propagation constant on the conductivity [36]. Nevertheless, we expect it to be helpful for clarifying the origin of extra features in Fig. 6.

According to the aforementioned expressions, the minima of the in-plane EM field should appear at  $w_n \approx n\lambda/2$  for integer values of  $n$ , whereas the condition for constructive interference is fulfilled for

$$w_m \approx \frac{\lambda}{4\pi} (\arccos\{-\text{Re}[\varphi]/|\varphi|^2\} + 2\pi m) \quad (18)$$

with  $\varphi = (1 - Z_s)/(1 + Z_s)$  and  $m$  also being an integer. Notice that the latter equation is no more than the SIBC version of the criterion about the number of nodes in groove cavity modes previously presented in [28]. In order to check the validity of such estimates we present in Fig. 7 the dependence on groove depth of the scattering magnitudes calculated at the resonant wavelength  $\lambda = 619$  nm ( $k_p d = 2\pi$ ) for two very dif-

ferent groove widths and the same  $N, d$  as in Fig. 6. As can be seen, the positions of maxima and minima are very well described by the analytical expressions for the purely academic case with  $a = 10$  nm. With respect to that of  $a = 100$  nm, we have to stress that the condition for “invisibility” is still in good agreement with the lowest mode approximation. Of course, the relative weight of in-plane and out-of-plane scattered energy does not depend on groove depth in a such trivial way, but LMA provides a starting point for a further optimization of SPP scattering devices.

### 3.4 Directionality properties of the emitted light

One of the possible applications of finite arrays of indentations lies in their capability to convert SPPs into light. Therefore, it is worth studying the directionality properties of the emitted light in the system analyzed throughout this paper. For that purpose, we find it helpful to write the total out-of-plane scattered energy  $S$  at a given wavelength  $\lambda$  in the following form

$$S(\lambda) = \int_{-\pi/2}^{\pi/2} d\theta D(\theta), \quad (19)$$

where  $D(\theta)$  is the differential reflection coefficient (DRC), which provides the angular dependence of the radiated energy. In addition to this, we can also define a normalized DRC as  $\tilde{D}(\theta) \equiv D(\theta)/S$ . This auxiliary magnitude describes the sole spatial distribution of  $S$  without considering its integrated value.

Figure 8 shows the calculated  $\tilde{D}(\theta)$  for the two emittance maxima at the low-energy edges of the gaps ( $\lambda = 665$  nm and  $\lambda = 500$  nm) in Fig. 4(c), as well as for the two associated reflectance maxima ( $\lambda = 510$  nm and  $\lambda = 438$  nm). The distributions corresponding to the gap labelled with  $m = 2$  (solid and dashed curves) are beamed close to the normal. On the

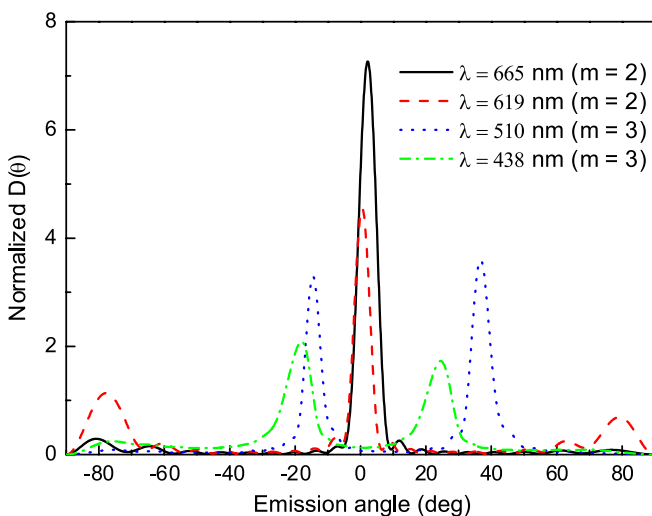


**FIGURE 8** Normalized DRC for an array of grooves with the same  $a, d, w$ , and  $N$  as in Fig. 4c. The wavelengths of the incident radiation corresponds to that of the  $R, S$  maxima at the edges of the SPP band-gaps in Fig. 4d:  $\lambda = 665$  nm (solid line),  $\lambda = 619$  nm (dashed line) for  $m = 2$  and  $\lambda = 510$  nm (dotted line), and  $\lambda = 438$  nm (dash-dotted line) for  $m = 3$

contrary, the ones coming from the gap with  $m = 3$  (dotted and dash-dotted curves) are beamed at higher angles. Notice that, at the condition of  $k_p d = m\pi$ ,  $\{E_\alpha\}$  are proportional to  $(-1)^{m\alpha}$ . Consequently, the radiated energy is sent out mainly at the normal direction for even  $m$  and close to tangent for odd  $m$ .

## 4 Summary

In this paper we have studied the scattering properties of a sub-wavelength periodic array of rectangular grooves in the visible and near IR ranges by means of a multimodal expansion technique. We have found that, associated with the low- $\lambda$  edge of the SPP band gap, the array behaves as a mirror (up to 80% reflectance for typical experimental values) whereas at the high- $\lambda$  edge, most of the light carried out by the SPP can be converted into collimated light (up to 90%). We have also shown that this resonant behavior can be achieved with a small number ( $\sim 5-10$ ) of indentations and it is generally quite robust with respect to variations in the groove depth. However, particular values of  $w$  can either increase or suppress the scattering efficiency of the whole structure. In our opinion, such a depth-tuning clearly constitutes a stimulating challenge for SPP-scattering devices.

**ACKNOWLEDGEMENTS** Financial support by the EU (projects FP6-NMP4-CT-2003-505699 and FP6-2002-IST-507879) and Spanish MEC (project MAT2005-06608-C02-02) is gratefully acknowledged.

## REFERENCES

- 1 H. Raether, *Surface Plasmons* (Springer, Berlin Heidelberg, 1988)
- 2 See, for example, W.L. Barnes, A. Dereux, T.W. Ebbesen, *Nature (London)* **424**, 824 (2003) and references therein
- 3 S.A. Maier, *Curr. Nanosci.* **1**, 17 (2005)
- 4 M.U. González, J.-C. Weeber, A.-L. Baudrion, A. Dereux, A.L. Stepanov, J.R. Krenn, E. Devaux, T.W. Ebbesen, *Phys. Rev. B* **72**, 161405 (2006)
- 5 J.C. Weeber, Y. Lacroute, A. Dereux, E. Devaux, T.W. Ebbesen, M.U. González, A.-L. Baudrion, *Phys. Rev. B* **70**, 235406 (2004)
- 6 J.R. Krenn, H. Ditlbacher, G. Schider, A. Hohenau, A. Leitner, F.R. Aussenegg, *J. Microsc. Oxford* **209**, 167 (2003).
- 7 J.C. Weeber, J.R. Krenn, A. Dereux, B. Lamprecht, Y. Lacroute, J.P. Goudonnet, *Phys. Rev. B* **64**, 045411 (2001)
- 8 S.I. Bozhevolnyi, V.S. Volkov, E. Devaux, J.-J. Laluet, T.W. Ebbesen, *Nature* **440**, 508 (2006)
- 9 J. Gómez-Rivas, M. Kuttge, H. Kurz, P. Haring Bolivar, J.A. Sánchez-Gil, *Appl. Phys. Lett.* **88**, 082106 (2006)
- 10 F. Pincemin, A.A. Maradudin, A.D. Boardman, J.J. Greffet, *Phys. Rev. B* **50**, 15261 (1994)
- 11 O.J.F. Martin, C. Girard, A. Dereux, *Phys. Rev. Lett.* **74**, 526 (1995)
- 12 T. Søndergaard, S.I. Bozhevolnyi, *Phys. Rev. B* **67**, 165405 (2003)
- 13 T. Søndergaard, S.I. Bozhevolnyi, *Phys. Rev. B* **69**, 045422 (2004)
- 14 T. Søndergaard, S.I. Bozhevolnyi, *Phys. Rev. B* **71**, 125429 (2005)
- 15 B.T. Draine, *Astrophys. J.* **333**, 848 (1988)
- 16 A.B. Evlyukhin, S.I. Bozhevolnyi, A.L. Stepanov, J.R. Krenn, *Appl. Phys. B* **84**, 29 (2006)
- 17 A.B. Evlyukhin, S.I. Bozhevolnyi, *Laser Phys. Lett.* **3**, 396 (2006)
- 18 F. Toigo, A. Marvin, V. Celli, N.R. Hill, *Phys. Rev. B* **15**, 5618 (1977)
- 19 A.V. Zayats, I.I. Smolyaninov, A.A. Maradudin, *Phys. Rep.* **408**, 131 (2005)
- 20 J.A. Sánchez-Gil, *Appl. Phys. Lett.* **73**, 3509 (1998)
- 21 J.A. Sánchez-Gil, A.A. Maradudin, *Phys. Rev. B* **60**, 8359 (1999)
- 22 J.A. Sánchez-Gil, A.A. Maradudin, *Appl. Phys. Lett.* **86**, 251106 (2005)
- 23 V.I. Tatarskii, *J. Opt. Soc. Am. A* **12**, 1254 (1995)
- 24 A.V. Shchegrov, I.V. Novikov, A.A. Maradudin, *Phys. Rev. Lett.* **78**, 4269 (1997)
- 25 F. López-Tejiera, F.J. García-Vidal, L. Martín-Moreno, *Phys. Rev. B* **72**, 161405(R) (2005)

- 26 J.D. Jackson, *Classical Electrodynamics*, 2nd edn. (Wiley, New York, 1975)
- 27 J. Bravo-Abad, F.J. García-Vidal, L. Martín-Moreno, *Phys. Rev. Lett.* **93**, 227 401 (2004)
- 28 F.J. García-Vidal, H.J. Lezec, T.W. Ebbesen, L. Martín-Moreno, *Phys. Rev. Lett.* **90**, 213 901 (2003)
- 29 A.Y. Nikitin, F. López-Tejeira, L. Martín-Moreno, *Phys. Rev. B* **75**, 035 129 (2007)
- 30 H. Lochbihler, R. Depine, *Appl. Opt.* **32**, 3459 (1993)
- 31 C. Wang, C. Du, X. Luo, *Phys. Rev. B* **74**, 245 403 (2006)
- 32 C. Sönnichsen, A.C. Duch, G. Steininger, M. Koch, G. von Plessen, J. Feldmann, *Appl. Phys. Lett.* **76**, 140 (2000)
- 33 E. Devaux, T.W. Ebbesen, J.C. Weeber, A. Dereux, *Appl. Phys. Lett.* **83**, 4936 (2003)
- 34 L. Yin, V.K. Vlasko-Vlasov, A. Rydh, J. Pearson, U. Welp, S.-H. Chang, S.K. Gray, G.C. Schatz, D.E. Brown, C.W. Kimball, *Appl. Phys. Lett.* **85**, 467 (2004)
- 35 A. Agrawal, H. Cao, A. Nahata, *New J. Phys.* **7**, 249 (2005)
- 36 J.R. Suckling, A.P. Hibbins, M.J. Lockyear, T.W. Preist, J.R. Sambles, C.R. Lawrence, *Phys. Rev. Lett.* **92**, 147 401 (2004)
- 37 S.C. Kitson, W.L. Barnes, J.R. Sambles, *Phys. Rev. Lett.* **77**, 2670 (1996)
- 38 S.I. Bozhevolny, A. Boltasseva, T. Søndergaard, T. Nikolajsen, K. Leosson, *Opt. Commun.* **250**, 328 (2005)